KEY ISSUES REVIEW

Physics approaches to the spatial distribution of immune cells in tumors

IOP Publishing Reports on Progress in Physics
Rep. Prog. Phys. **84** (2021) 022601 (18pp) https://doi.org/10.1088/1361-6633/abcd7b

Key Issues Review

Physics approaches to the spatial distribution of immune cells in tumors

Clare C Yu[1,2,*], Juliana C Wortman[1,8], Ting-Fang He[2,8], Shawn Solomon[2], Robert Z Zhang[2], Anthony Rosario[2], Roger Wang[2], Travis Y Tu[2], Daniel Schmolze[3], Yuan Yuan[4], Susan E Yost[4], Xuefei Li[5], Herbert Levine[5,6], Gurinder Atwal[7] and Peter P Lee[2]

[1] Department of Physics and Astronomy, University of California, Irvine, Irvine, CA 92697, United States of America
[2] Department of Immuno-Oncology, City of Hope Comprehensive Cancer Center and Beckman Research Institute, 1500 East Duarte Road, Duarte, CA 91010, United States of America
[3] Department of Pathology, City of Hope Comprehensive Cancer Center, 1500 East Duarte Road, Duarte, CA 91010, United States of America
[4] Department of Medical Oncology and Therapeutics Research, City of Hope Comprehensive Cancer Center, 1500 East Duarte Road, Duarte, CA 91010, United States of America
[5] Department of Bioengineering and the Center for Theoretical Biological Physics, Rice University, Houston, TX 77030, United States of America
[6] Department of Bioengineering and Department of Physics, Northeastern University, Boston, MA 02115, United States of America
[7] Cold Spring Harbor Laboratory, Cold Spring Harbor, NY 11724, United States of America

E-mail: cyu@uci.edu

Received 1 November 2019, revised 3 November 2020
Accepted for publication 24 November 2020
Published 26 January 2021

Abstract

The goal of immunotherapy is to mobilize the immune system to kill cancer cells. Immunotherapy is more effective and, in general, the prognosis is better, when more immune cells infiltrate the tumor. We explore the question of whether the spatial distribution rather than just the density of immune cells in the tumor is important in forecasting whether cancer recurs. After reviewing previous work on this issue, we introduce a novel application of maximum entropy to quantify the spatial distribution of discrete point-like objects. We apply our approach to B and T cells in images of tumor tissue taken from triple negative breast cancer patients. We find that the immune cells are more spatially dispersed in good clinical outcome (no recurrence of cancer within at least 5 years of diagnosis) compared to poor clinical outcome (recurrence within 3 years of diagnosis). Our results highlight the importance of spatial distribution of immune cells within tumors with regard to clinical outcome, and raise new questions on their role in cancer recurrence.

Keywords: cancer, tumor microenvironment, maximum entropy, fractal dimensions, spatial distribution, immune cells, tumor infiltrating lymphocytes

(Some figures may appear in colour only in the online journal)

*Author to whom any correspondence should be addressed.
[8]JCW and T-F H contributed equally to this work.
Corresponding editor: Professor Jose Onuchic.

1. Introduction

1.1. Why should physicists work on cancer?

Why should physicists pay attention to cancer as a research topic? Traditionally, cancer research has been the purview of biologists and medical researchers. Yet, despite the billions of dollars that have been spent on the war on cancer, far too many people are still battling this disease. Consider the following statistics. Worldwide, in 2018, approximately 18 million new cases of cancer were diagnosed and 9.6 million people died of cancer (17% of deaths) [1]. In the United States alone about 600 000 people die of cancer each year [2]. This accounts for 1 in 4 deaths. It is estimated that during their lifetime, one in two men and one in three women will be diagnosed with cancer [3]. These statistics highlight the need for new ways of thinking.

As a result, interdisciplinary collaborations of cancer researchers, physicists, mathematicians, engineers and computer scientists have been working to hasten progress with new techniques and different approaches. There have been efforts in both the public and private sector to encourage physicists, mathematicians and engineers to collaborate with cancer researchers and clinical oncologists (medical doctors specializing in cancer). For example, the National Cancer Institute sponsors a Physical Sciences Oncology Network, and Stand Up to Cancer sponsors interdisciplinary convergence teams consisting of theoreticians and oncologists. Since cancer mortality is still high, the hope is that new perspectives and approaches from other fields could lead to new discoveries.

Traditionally, physicists have developed tools that are commonly used to screen, diagnose and treat cancer such as x-rays, ultrasound, radiation therapy, and magnetic resonance imaging (MRI). Even now, physicists are advancing technologies to help in the fight against cancer. These include ultra-low field MRI that holds the promise of cheaper MRI machines with much better contrast than high field MRI that could image prostate cancer, for example [4]. (Contrast refers to the ability to differentiate between different types of tissue, e.g., bone, fat, muscle, etc.) Prostate cancer is typically a heterogeneous mixture of healthy and cancerous cells rather than a well defined solid tumor, making it a challenge to image with current clinical high field MRI [4]. Another example is lab-on-a-chip microhabitats that can be used for *in vitro* models of 3D tumors with functioning blood vessels [5]. Nanofabricated microhabitats such as these and others enable anti-cancer drugs to be screened as well as providing a platform to study drug resistance [6, 7].

Computer simulations and analytic calculations, tools common to theoretical physicists, are being increasingly applied, sometimes to great effect, in cancer research. Historically, in 1943, the physicist, Max Delbruck, worked out the statistical distribution of mutant cells to explain Salvador Luria's observations of bacterial resistance to viral infections [1943]. These equations still help to predict how cancers develop chemotherapy resistance. In the 1970s, Larry Norton and Richard Simon showed that tumor growth obeys Gompertz' law which means that tumors do not simply grow exponentially forever but tend to grow slower as they get larger [9]. This led them to formulate the Norton–Simon hypothesis that the rate at which a tumor shrinks in response to chemotherapy is proportional to what its growth rate would have been had that tumor been left untreated at that size [10, 11]. This concept suggests that tumors given less time to regrow between treatments are more likely to be destroyed. This led to an approach to chemotherapy called sequential, dose-dense treatment which is now an international standard of care [12–14].

Although mathematical modeling continues to guide chemotherapy regimens [15], it has a much wider range of applicability to cancer-related problems. For example, using the principles of evolutionary biology, modeling has been used to study tumor initiation, growth and response to treatment [16, 17]. Another example is the use of evolutionary game theory to study strategic interactions between cancer and stromal cells without needing a detailed understanding of signaling pathways [18, 19]. Game theory has also been applied clinically to administer adaptive therapies [20, 21].

Aside: let us pause a moment to explain some terms in the previous paragraph. A signaling pathway is a sequence of switches in a cell in which protein A activates or deactivates protein B that in turn switches protein C on or off, etc. A tumor is more than just a collection of cancer cells. The cancer cells typically cluster in cancer cell islands about 100 microns in diameter that are surrounded by stroma consisting of collagen fibers, blood vessels, and various types of cells. We will describe this further below.

In addition to tools, physicists bring a different perspective that can provide a broader context for viewing cancer. Cancer research typically focuses on signaling pathways that have been over-activated or deactivated due to gene mutations. These aberrant signaling pathways enable a tumor to grow and spread. Regarding the tumor microenvironment (TME) (described below) more holistically, some of these signaling pathways can be viewed as part of the mechanobiology of tumors. Cells sense the stiffness of their surroundings, e.g., through proteins that link the cell to other cells or to the extracellular matrix, and this can cause cancer cells to proliferate, change their shape, or move through various signaling pathways [16, 22]. Cells in the tumor can respond by remodelling their microenvironment to make it stiffer by increasing the density of collagen fibers so that the tumor becomes a 'lump'. This stiffness can be measured with tools such as ultrasound, magnetic resonance elastography [23], sensitive microindenters [24], and atomic force microscopy indentation [25]. Cancer cells themselves can become stiffer or softer than normal cells, and this can be measured with a variety of techniques such as magnetic bead rheology [26, 27], optical tweezer manipulation of beads attached to cells [28], scanning force microscopy [29, 30] and an optical stretcher that uses the momentum transfer from opposing laser beams to deform a cell [29, 31]. Softer, more deformable cancer cells enhance their motility and ability to metastasize (spread to other organs) [29] which can be further enhanced by using collagen fibers as tracks along which to migrate [32].

Not only the rheology of cells but also their shape can give insight into their motility. By drawing an analogy to transitions

between jammed and unjammed collections of packed objects, Lisa Manning and her collaborators have quantitatively shown that cells with a larger aspect ratio are more motile while those with a smaller aspect ratio are jammed [33–35]. This is an example of how concepts from physics can bring new perspectives to cancer research.

Physical concepts can also provide organizing principles. For example, cancer can be considered from the viewpoint of the breakdown of regulation of mass transport at different length scales with metastasis and tissue invasion being at the cell-tissue level and signaling molecules enabling rogue signaling pathways being at the intracellular level [16, 36]. (Explanation of tissue invasion: epithelial cells line the inner surfaces of tubes and cavities in the body, e.g., the lungs and gastrointestinal tract. Carcinomas are cancers that originate from epithelial cells. Invasive carcinomas refer to cancer cells that break through the basement membrane, a tough sheath of tissue that underlies the epithelial cells, and that invade tissue where epithelial cells do not belong.)

In short, physicists collaborating with cancer researchers can bring experimental and theoretical tools as well as new ideas that provide unifying principles and a broader perspective. These have the potential to open new avenues of inquiry. In addition physicists bring a cultural ethos that can promote more quantitative and reproducible measurements. About 90% of preclinical cancer research results are not reproducible [37]. The biotech company Amgen tried to confirm the results of fifty-three landmark studies and found that they could only confirm the scientific findings in six cases (11%). In the cases where the results could not be reproduced, the investigators often presented the results of only one experiment rather than findings that were reflective of the entire data set. Amgen's findings are consistent with other studies. For example, Bayer HealthCare in Germany reported that only about 25% of published preclinical studies could be validated [38]. 70% of the studies analyzed by Bayer involved cancer research, some of which might have also been analyzed in the Amgen study.

A greater exchange of research information before publication could also help to hasten progress. For example, in physics, there is an online preprint archive (https://arxiv.org) where researchers post preprints before publication. Unfortunately, even though such an archive exists in biology (www.biorxiv.org), many biologists are not interested in utilizing such an archive [39]. One reason is that some biologists are afraid of other researchers stealing their results, which is rather ironic given the poor track record of reproducibility of biological research results [37, 38].

Current cancer research focuses on developing therapeutics that target signaling pathways on which the growing tumor depends. Yet, all too often these chemotherapy drugs, combined with surgery and radiation, provide only a temporary fix as the cancer develops resistance and recurs [40]. This resistance can come from a variety of sources, e.g., cancer cells can develop mutations that render a particular chemotherapy drug ineffective, or poorly organized blood vessels in the tumor can compromise the delivery of chemotherapy drugs as well as oxygen to some cancer cells [41, 42]. In the latter case, the lack of oxygen (hypoxia) can increase resistance to chemotherapy and radiation treatment as well as impair the immune response to cancer [41, 42].

In recent years, a paradigm shift has occurred. Rather than using drugs to kill the cancer, immunotherapy mobilizes the immune system to kill cancer cells. Immunotherapy is more effective when the immune cells recognize the cancer and infiltrate the tumor. In fact, for some types of cancer, the prognosis is better when the density of killer T cells (that can kill cancer cells) is higher in the tumor, even if no immunotherapy is employed. We will discuss this more below, but suffice it to say that while immunotherapy has shown promising results, we are still a long way from curing cancer.

As Robert Austin has pointed out [43], such failure means that we just do not understand the basic principles behind cancer. We must think more broadly and physicists can help to expand the way we approach cancer. For example, an exclusive focus on signaling pathways and gene mutations ignores the physical characteristics of tumors. In particular, it ignores the spatial aspects of tumors, e.g., the spatial organization of cells and structures. Such spatial structure can affect the ways cells interact with each other and the structures in their environment. Studies on the spatial aspects of tumors could lead to different approaches and treatments.

In this article, after an overview of cancer, immunology and immunotherapy, we give examples of how techniques used by physicists can be applied to quantify the spatial distribution of immune cells in tumors. These techniques include fractal dimensions and maximum entropy.

1.2. Epidemiology of breast cancer

Since the rest of this article will focus on breast cancer, we begin with some breast cancer statistics. According to the most recent Global Cancer Statistics (GLOBOCAN 2018), breast cancer represented 11.6% of all cancers in 2018, making it the second most commonly occurring cancer after lung cancer, and the cause of 6.6% of total cancer deaths worldwide [44]. In 2020 in the United States, it is estimated that over 270 000 women will be diagnosed with invasive (stage 1 and higher) breast cancer; about 50 000 women will be diagnosed with *in situ* (stage 0) breast cancer; about 40 000 women will die of breast cancer; and about 2000 men will be diagnosed with breast cancer [45].

One of the more aggressive types of breast cancer is triple negative breast cancer (TNBC). TNBC cells lack appreciable expression of three receptors of ligands that promote growth of cancer cells. (Receptors are proteins on the surface of the cell that bind to specific molecules called ligands.) These three receptors are hormone epidermal growth factor receptor 2 (HER-2), estrogen receptors (ER) and progesterone receptors (PR). TNBC occurs in 15%–20% of breast cancer cases. According to a recent study of TNBC, 76.2% of recurrences occurred within the first 5 years after surgery, with the median time of recurrence of 2.7 years [46]. We mention this type of breast cancer because some of the results below involve TNBC patients.

1.3. Importance of the tumor microenvironment

As we mentioned above, tumors do not consist solely of cancer cells because they need a supportive environment known as the TME in order to survive and thrive [47]. The TME can be thought of as an ecosystem consisting of blood vessels, lymph vessels (see below), various types of immune cells, fibroblasts, extracellular matrix, etc. (Fibroblasts are cells that synthesize extracellular matrix and fibers such as collagen; fibroblasts are the most common cells in connective tissue.)

The evolution and progression of cancer depends on the TME. For example, the TME can play an important role in tumorigenesis, i.e., in the formation of tumors [48]. In particular, damage to the TME can cause pre-malignant cells to become malignant [48–51]. For example, injecting a cancer-causing virus (Rous sarcoma virus) into the wing of a chicken produces a tumor at the injection site but not elsewhere, even though the virus has spread throughout the chicken. If the other wing is then wounded, a tumor is formed at the site of the wound [49]. In another experiment [50], pre-malignant cells (COMMA-D mammary epithelial cells with p53 mutations) placed on previously irradiated tissue (mammary fat pads in mice) were about four times more likely to form tumors than when the cells were placed on non-irradiated tissue. Furthermore, the tumors on the irradiated tissue were significantly larger and grew more quickly than those on the non-irradiated tissue. One reason that damaging the TME promotes tumorigenesis is that the growth factors (signaling proteins like TGF-β) that are produced as part of the wound-healing process also promote the inception and growth of tumors [52] as well as metastasis [53].

Lymph vessels are another component of the TME and can be thought of as a sewage system for cells. Cells are bathed in interstitial fluid from which they absorb nutrients and into which they dump waste. Lymph vessels take up interstitial fluid and conduct it to lymph nodes. The fluid inside lymph vessels is referred to as lymph. Eventually lymph is conveyed to blood vessels (veins). The lymphatic system is much more than just a waste removal system; it is an important part of the immune system as we describe below.

2. Introduction to how lymphocytes fight cancer

Immunology is a fascinating and complex field of study. A good introductory text is [54] and much of what follows in this section comes from that book. Here we will only give a few brief facts to equip the reader with what will be needed to follow this article. White blood cells are immune cells. In this article we will focus on lymphocytes which are a subset of white blood cells. The two main categories of lymphocytes are T cells and B cells. B cells are best known for producing antibodies, which are proteins that recognize and attach to antigens, e.g., a specific protein on invading bacteria or viruses. The antibody tags the invader for destruction by other cells in the immune system, e.g., macrophages. The B cells that specialize in producing antibodies are called plasma cells. However, B cells can perform other functions such as presenting antigens for (helper) T cells to inspect, and secreting cytokines which are chemical signaling molecules that direct the actions of other immune cells.

T cells only recognize antigens in the form of pieces of proteins called epitopes that are displayed on the surface of antigen presenting cells (APCs) in 'display cases' that are called major histocompatibility complexes (MHCs). You can think of an MHC as a hot dog bun and the epitope as the hot dog [54]. The surfaces of T cells have T cell receptors (TCRs) which are antibody-like protein complexes that recognize and bind to their cognate antigens, i.e., specific epitopes in the MHCs. In general, the TCRs on different T cells will recognize different antigens just as the locks on front doors of different houses require different keys. There are three main types of T cells: killer T cells (cytotoxic T lymphocytes or CTLs), helper T cells, and regulatory T cells. Cytotoxic T cells are able to kill unwanted cells, e.g., cancer cells and virus-infected cells. Helper T cells (Th cells) secrete cytokines and help activate CTLs and B cells. Regulatory T cells suppress the immune system in order to keep it from overreacting or from acting inappropriately. In the lab, these different types of T cells can be distinguished by specific protein complexes on their surfaces. In particular, cytotoxic T cells and helper T cells express CD8 and CD4 co-receptors, respectively, on their surface. So we sometimes refer to killer T cells as $CD8^+$ T cells, and helper T cells as $CD4^+$ T cells. The plus sign in the superscript means that these cells stain positive for these protein markers by binding with their respective color-coded antibodies in the immunostaining process.

Lymph nodes are small bean-shaped structures where immune cells (such as T cells, B cells and APCs that present antigens to certain lymphocytes such as T cells) meet and communicate. B cells and T cells that find their cognate antigens in lymph nodes can also be activated there. Lymph nodes are highly organized with B cells congregating together with other B cells in a region called the cortex while T cell aggregate together with other T cells in the paracortex (which is adjacent to the cortex).

Lymphocytes must be activated before they can function. Activation requires recognition of the B or T cell's cognate antigen followed by a second, or co-stimulatory, signal. For example, to activate a helper T cell, its TCR must bind to its cognate antigen displayed by an APC which could be a dendritic cell, a B cell or a macrophage. The co-stimulatory signal consists of a protein on the surface of the APC, e.g., B7, binding to a receptor, e.g., CD28, on the surface of the Th cell. Once the Th cell is activated, it proliferates, produces cytokines to help direct other immune cells, and helps activate other immune cells, e.g., B cells and cytotoxic T cells.

In order to kill cancer cells, activated cytotoxic T cells (or effector CTLs) must infiltrate the tumor and find their cognate antigens expressed on cancer cells. These cancer antigens are unique to cancer cells and appear foreign to the immune system; they are often referred to as neoantigens. Tumors with cancer cells that have many mutations have a greater chance of producing neoantigens that can be recognized by the immune system. For example, melanoma (a type of skin cancer) tends to have a high mutational burden. Tumor mutational burden can be measured in units of number of mutations

per megabase (10^6 bases). Melanoma tumors typically have a median mutational burden of 10 mutations per megabase [55].

Cancer cells can evade detection and destruction by killer T cells in a variety of ways such as mutating to prevent their antigens from being presented or recognized by cytotoxic T cells, or by promoting an environment that suppresses the immune system, e.g., by emitting various cytokines [56] or by rapid consumption of the amino acid tryptophan to starve killer T cells of tryptophan. Cancer cells can also restrain CTLs from killing and proliferating by expressing ligands for immunosuppressive receptors (checkpoint proteins) on killer T cells. For example, one of these checkpoint protein receptors found on the surface of CTLs is called programmed cell death 1 (PD-1). When the ligand for PD-1, which is called programmed cell death ligand 1 (PD-L1), binds to PD-1, the killer T cell does not function very well. Cancer cells with PD-L1 basically have a 'key' or ligand that can effectively neutralize killer T cells by inserting the PD-L1 'key' into the 'lock' or receptor. Thus the cancer cells can prevent the killer T cells from killing the cancer cells. As we will see below, one immunotherapy strategy is to block ligation of checkpoint proteins.

3. Introduction to immunotherapy

Currently, there is a great deal of interest in treating cancer by using immunotherapy to mobilize the immune system to kill cancer cells. We describe below some ways in which this is being done. (For more details, see [54].)

Monoclonal antibodies are antibodies produced in the laboratory that target specific proteins on the surface of cells. For example, some particularly aggressive types of breast cancer cells express high amounts of a growth factor receptor called HER2. When growth factor proteins bind to (or ligate) this surface receptor, the cancer cells proliferate. The monoclonal antibody Herceptin (trastuzumab) can bind to the HER2 receptor and prevent the growth factor proteins from ligating the receptor, thus blocking the growth signals and slowing growth. In combination with chemotherapy, Herceptin has proven to be an effective treatment of HER-2 positive breast cancer, i.e., breast cancer which overexpresses the hormone receptor HER-2 [3].

3.1. Checkpoint inhibitors: antibodies that block the ability of cancer cells to turn off killer T cells

Checkpoint inhibitors are monoclonal antibodies that are used to interrupt the way that cancer cells deactivate killer T cells. As we mentioned above, activated cytotoxic T cells express 'checkpoint' protein receptors on their surface that, when ligated, suppress the activity of CTLs. In particular, a cancer cell can express PD-L1 on its surface and bind this ligand to a PD-1 receptor on a CTL to prevent being killed by a cytotoxic T cell. Checkpoint inhibitors are monoclonal antibodies that bind to, e.g., PD-1 or PD-L1, thus preventing the cancer cell from deactivating the killer T cell. It is analogous to taping over the keyhole or wrapping tape around the key so that the key cannot go into the keyhole.

A number of checkpoint inhibitors are being used clinically to treat several different types of cancer [57]. Immunotherapy that blocks the binding of PD-1 to PD-L1 works best if the tumor cells express large amounts of PD-L1, as in Hodgkin's lymphoma where the response rate approaches 90% [54]. However, for other types of cancers, the response rate is about 20%–40% [54, 56, 58]. Checkpoint inhibitors tend to be more effective in cancers with a high mutational load such as melanoma because these have a greater chance of activating CTLs. Breast cancer, on the other hand, has a more moderate mutational load with a median of about 1 per megabase [55]. However, the immunogenicity of breast cancer, i.e., its ability to induce an immune response, is heterogeneous and depends on the subtype of breast cancer [59]. Among the various types of breast cancer, TNBC tends to have the highest concentration of tumor infiltrating lymphocytes (TILs) which is an important indicator of response to immunotherapy [60, 61]. Indeed, TNBC patients whose tumors expressed PD-L1 had a median survival time that was 7 months longer when treated with a monoclonal antibody (atezolizumab) that bound to PD-L1 plus chemotherapy (nab-paclitaxel) compared to patients treated with chemotherapy alone [60, 62]. (There was no benefit for patients whose tumors did not express PD-L1.) Hope Rugo speculated that chemotherapy may improve response to immunotherapy by making the tumor look more foreign [60].

3.2. CAR T cell therapy: engineering T cell receptors

As we mentioned earlier, T cells have TCRs that bind to specific antigens. The TCRs on a given T cell are all identical and recognize one specific antigen which is referred to as the TCR's cognate antigen. Different T cells have different TCRs. If the TCRs on a T cell recognize and bind to their cognate antigen, the T cell proliferates, i.e., divides to produce daughter cells with identical TCRs. CAR T cell therapy is a rapidly emerging cancer treatment in which the TCR is artificially engineered to recognize antigens on cancer cells. CAR stands for 'chimeric' antigen receptor. (Chimera was a beast in Greek mythology that had the head of a lion, the body of a goat and a serpent's tail.) The receptors on CAR T cells are designed to recognize and bind to specific surface proteins. It is important to note that these CAR T cognate antigens need not be presented by MHC molecules [54]. Cells that display these cognate proteins are then destroyed by the CAR T cells. CAR T cell therapy has been most successful in treating blood cancers such as leukemia and lymphoma.

Cancer immunotherapy is still in its infancy and a wide variety of strategies are being investigated to boost the immune response and suppress tumor evasion of the immune system [56]. These include oncolytic (cancer killing) viruses [63], neoantigen vaccines [64, 65], and local tumor hyperthermia (heating) to boost immune cell response and make the tumor more susceptible to immune attack [66, 67].

3.3. Spatial distribution of immune cells

Immunotherapy is more effective when lymphocytes recognize cancer antigens and invade tumors. This is why a high

density of TILs is indicative of a better response to checkpoint inhibitors [68–71]. However, even for patients that do not receive immunotherapy, a high density of TILs is associated with a good prognosis in several types of cancers [72–74]. For example, higher densities of $CD3^+$ and $CD8^+$ T cells were associated with a lower rate of recurrence in colorectal carcinoma [75]. (CD3 is a marker for all T cells and CD8 is a marker for cytotoxic (killer) T cells.) In the case of patients with triple negative and HER2-positive breast cancers, a higher density of TILs is associated with a better prognosis [61]. While the prognostic value of the density of $CD3^+$ and $CD8^+$ T cells infiltrating tumors is well known, the clinical significance of other types of immune cells, such as B cells, is less clear [76, 77].

Averaging cell densities over the entire tissue overlooks the spatial heterogeneity in the distribution of TILs within the tumor which may be clinically important [78–80]. If we view the TME in ecological terms, interactions between the different components of this ecosystem depend upon their spatial organization. Regional differences in selective pressures produce microhabitats resulting in phenotypic and genetic heterogeneity [81, 82]. (Phenotype refers to the set of observable characteristics.) So it is worth considering whether the spatial distribution of TILs is associated with a difference in clinical outcome, i.e., in whether or not the cancer recurs.

In the following sections, we will describe ways to quantify the spatial distribution of immune cells. This will consist of a review of techniques found in the research literature as well some techniques that we have developed. It turns out that the spatial distribution of lymphocytes is indeed clinically significant. In particular, we find that TILs are more spread out in tumors of patients who do not experience a recurrence of TNBC while the TILs tend to be more clustered in cases where cancer recurs. This leads to the open question of what factors determine the spatial distribution of lymphocytes. Answering this question could lead to new immunotherapy strategies. Regarding the techniques to measure the spatial distribution, these may some day be useful as prognostic indicators to give the probability of cancer recurrence. If used in conjunction with clinical trials of new therapeutics, these techniques may be able to indicate which patients will likely respond to a given treatment. Since immunotherapy can be quite expensive and produce severe side effects, having ways to decide which patients are good candidates for a certain therapy could be valuable.

3.4. Review of previous work on the spatial distribution of immune cells

So let us consider the problem of quantifying the spatial distribution (or arrangement) of cells in histology-based images with a single scalar number. (Histology is the study of the microscopic anatomy of tissues.) There have been a number of efforts to quantify spatial heterogeneity of the TME based on comparing populations of cells [83]. For example, the Morisita–Horn index, M, was used to quantify the spatial colocalization of tumor and immune cells, and it is defined as follows:

$$M = \frac{2\sum_i^R p_i^L p_i^c}{\sum_i^R \left(p_i^L\right)^2 + \sum_i^R \left(p_i^c\right)^2}, \tag{1}$$

where p_i^L and p_i^c are the fractions of immune cells and cancer cells within a region i, and the tumor has been divided into a total of R regions with $1 \leqslant i \leqslant R$ [83]. It was found that significant colocalization of tumor and immune cells was associated with a higher disease-specific survival in HER2-positive breast cancers [83, 84].

The Getis–Ord analysis [85] was used to locate immune hotspots where the clustering of immune cells was significantly above background [86]. The analysis divides an image of tumor tissue into n regions with a grid of squares and then assigns a z score to each region i using

$$z_i = \frac{\sum_{j=1}^n w_{i,j}c_j - \langle c\rangle \sum_{j=1}^n w_{i,j}}{\sqrt{\langle c^2\rangle - \langle c\rangle^2}\sqrt{\frac{\left[n\sum_{j=1}^n w_{i,j}^2 - \left(\sum_{j=1}^n w_{i,j}\right)^2\right]}{n-1}}}, \tag{2}$$

where c_j is the number of cancer cells or lymphocytes in region j; $\langle c\rangle$ is the average value of c, and $w_{i,j} = 1$ if regions i and j are neighbors and 0 otherwise. If the p-value (defined below) associated with z_i satisfies $p_i < 0.05$, then the region is considered a clustering hotspot. Colocalization occurs in regions that are hotspots for both immune cells and cancer cells. A combined immune-cancer hotspot score was found to be associated with good prognosis in ER-negative breast cancer [86].

A quantitative measure of the infiltration of immune cells into a tumor is the intratumor lymphocyte ratio (ITLR) which is defined as the ratio of the number of intratumor lymphocytes to the total number of cancer cells in a histological sample [87]. A high ITLR was found to be associated with good disease specific survival in ER-negative/HER2-negative breast cancer [87].

Natrajan *et al* [88] quantified the spatial heterogeneity in breast tumors with regard to the proportions of different cell types, e.g., cancer cells, lymphocytes and stromal cells, in different regions of the tumor by calculating the Shannon entropy in each tumor region:

$$d_j = -\sum_{i=1}^m p_i \log p_i, \tag{3}$$

where m is the number of cell types being considered and p_i is the fraction of the ith cell type in region j. The larger the value of the Shannon diversity index d_j, the more heterogeneous the environment in terms of the diversity of the cell types. Since the image was divided into n regions, the Shannon diversity index had a distribution of values. Natrajan *et al* [88] used Gaussian mixture models to fit the distribution of Shannon entropies. Their ecosystem diversity index (EDI) was the number of Gaussians needed to fit the distribution. They found that high EDI values were associated with high microenvironmental diversity and poor prognosis. Somewhat ironically, if most of the regions have high Shannon entropies such that a single Gaussian can be used to fit the distribution, then the EDI is low.

The irregular shape of tumors brings to mind fractals. Indeed, fractal dimensions (FDs) [89] have been used to characterize the irregular morphology of tumors [90–92] and vasculature [93, 94] as well as subcellular structures such as mitochondria [95] and nuclei [96]. There are numerous ways to calculate FDs. In the box counting method, the number N of squares (each with area L^2) needed to cover the 2D image of a tumor, say, is proportional to L^{-d}, where d is the FD in the limit that L goes to zero (or a very small value). The more irregular the shape of the tumor is, the higher the FD is and the poorer the prognosis [90, 91].

Assuming that the structure of tumor tissue is reflected in the arrangement of cancer cell nuclei, Waliszewski *et al* calculated several different FDs as well as the Shannon entropy and lacunarity to characterize the spatial distribution of cancer cell nuclei in prostate tumor tissue and compared the results to the corresponding Gleason scores in an attempt to find a more objective way to classify prostate tumor tissue [97, 98]. (Gleason scores are a way of grading prostate tumor tissue with higher scores corresponding to more abnormal tissue.)

3.5. Spatial distribution of immune cells across multiple length scales

The approaches described above produce measures of the spatial distribution at a single length scale. More recently, to move beyond this limitation, we developed several unique statistical approaches that use coarse graining to examine the spatial distribution of various types of cells and structures within the TME over a range of length scales [99].

Occupancy. The first technique is called 'occupancy'. We begin with an image of tissue where different types of cells are labeled, i.e., immunostained, with different colors, e.g., cytotoxic T cells are bright red, B cells are cyan, etc. We overlay the tissue image with a grid of squares as in figure 1. For each square, we then ask a binary (yes–no) question, e.g., 'is there at least one $CD20^+$ B cell in the square?' If the answer is yes, we assign a '1' to that square. If the answer is no, we assign a '0' to the square. The *occupancy* g is the fraction of squares with 1's, i.e., it is an estimate of the probability that a square will have a 1. To characterize the spatial distribution at different length scales, we varied the size of the squares in the grid and computed the occupancy as a function of L, the length of one side of a square. Note that the occupancy will be affected by the average cell density for questions such as 'is there at least one $CD20^+$ B cell in the square?' because the higher the average cell density, the higher the probability that a square is assigned a '1'. We can plot the occupancy averaged over patients or samples versus the square size L (see figure 2). We found that the area under the curve (AUC occupancy) differed between TNBC patients with good and poor clinical outcome for $CD20^+$ B cells and $CD8^+$ T cells. We defined patients with no recurrence within 5 years after surgery as good clinical outcome ($n = 24$) and patients who had recurrence within 3 years after surgery as poor clinical outcome ($n = 13$).

Thinning. As we mentioned above, occupancy tends to increase with the average cell density. One way to remove the effect of density on the occupancy is to reduce, or thin, the density by randomly eliminating cells, e.g., $CD8^+$ T cells, in the various images until the densities in all the tissue images have the same value as the image with the lowest density. Here is a simple example of how to randomly remove B cells. To randomly remove half the B cells from an image, you would go to each B cell, flip a coin, and remove the cell if you get 'heads' and keep the cell if you get 'tails'. Figures 2(C) and (D) show thinned plots of occupancy vs square size L. The difference in the area under the curves (AUC) between good and poor clinical outcomes is statistically significant for thinned B cells (p-value $= p = 8 \times 10^{-4}$) but not for thinned killer T cells (p-value $= p = 0.3$). This suggests that the spatial distribution, rather than the density, of B cells differs significantly between good and poor outcomes.

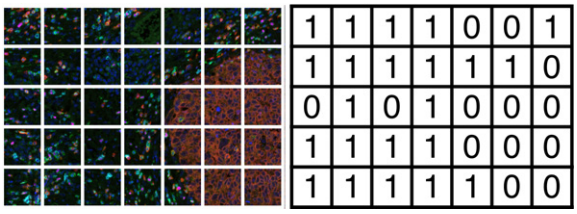

Figure 1. Grid of squares overlaying a tissue image. 1's (0's) correspond to yes (no) answer to the binary question asked of each square, e.g., 'is there at least one B cell in the square?' This is used for calculating occupancy, FDs, and FD differences.

P-value. In the previous paragraph we calculated the p-value under the null hypothesis to ascertain whether a quantity, such as the area under the curve, is clinically significant. The p-value is a standard statistical measure of a binary classifier [100]. Binary refers to our assumption that the clinical outcome is either good or poor. The p-value is the probability of obtaining a random sample with a mean at least as far from that of the null hypothesis as is observed, assuming the null hypothesis is true. In our case, the null hypothesis states that the result could arise by random chance. The smaller the p-value is, the greater the probability that the null hypothesis is not valid. In general, results are considered significant if $p < 0.05$.

Fractal Dimension. Another way to characterize the number of boxes with 1's and hence, the spatial distribution of cells, is with FD. Although a number of studies have used FD to analyze morphologies associated with tumors [90–96], we used it to quantify the spatial distribution of immune cells. While there are a number of different ways to define the FD, we chose to use a variation of the box counting method [101]. The number $n(L)$ of squares with '1' will be proportional to $(1/L^{\delta})$ where δ is one type of FD and L^2 is the area of a square. The constant of proportionality depends on the size of the tissue that dictates the number of boxes covering the tissue. To avoid this, we found it convenient to define the FD s as:

$$s(L) = -\frac{d\left[\log\left(n(L)\right)\right]}{d\left[\log\left(L\right)\right]} \tag{4}$$

(Note that unlike the more common definition of the box-counting FD, we do not take the limit $L \to 0$, because we are interested in the distribution of individual immune cells at different length scales.) We used a different variable, $s(L)$, rather

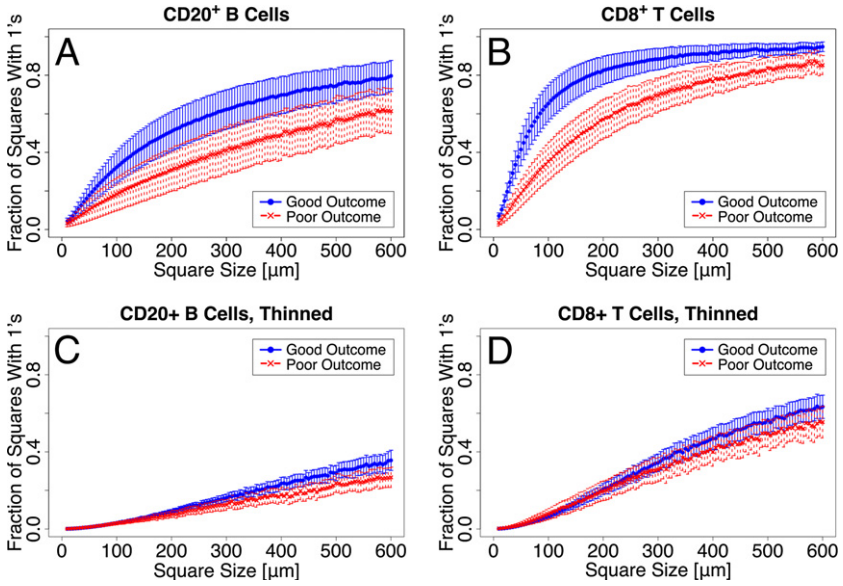

Figure 2. Occupancy for $CD20^+$ B cells and $CD8^+$ T cells vs square size before and after thinning. Thinning removes the effect of density. Notice that blue points (good outcome) are above red points (poor outcome) which indicates that the B and T cells are more spread out in good outcome. The error bars indicate 95% confidence intervals. (A) $CD20^+$ B cell occupancy before thinning (B) $CD8^+$ T cell occupancy before thinning (C) $CD20^+$ B cell occupancy after thinning the B cells to a density of 12 B cells mm^{-2} (D) $CD8^+$ T cells occupancy after thinning the T cells to a density of 25 $CD8^+$ T cells mm^{-2}.

than δ, since $n(L)$ typically does not follow a simple power law as L is varied (see below).

Both occupancy and FD depend on the number of squares with 1's, so there must be a simple relation between the dependence of occupancy on L and FD d. To find the relation, consider the following. Suppose the total number $N(L)$ of squares covering the image of the tissue goes as $(1/L^D)$. Then if

$$n(L) \sim \frac{1}{L^{\delta}}, \tag{5}$$

then the occupancy g will go as

$$g = \frac{n(L)}{N(L)} \sim L^{D-\delta}. \tag{6}$$

Note that D need not be equal to 2 since the image of the tissue may be irregular or there may be regions that were not imaged.

Fractal dimension difference. To see if cells are clustered or spread out, we looked at the difference Δs in FD between large and small length scales: $\Delta s = s_{\text{Large}} - s_{\text{small}}$, where s_{Large} is the FD at large length scales and s_{small} is the FD at small length scales. The small and large length scales should roughly bracket the typical, or median, nearest neighbor distance between cells of the same type, e.g., $CD8^+$ T cells. In all the cases we examined, $\Delta s > 0$. If Δs is large, it means that the cells are more dispersed, i.e., more spatially spread out because they appear to be more two-dimensional at large length scales and more zero-dimensional (point-like) at small length scales. (figure 3(A) uses illustrations to explain this concept.) If $\Delta s = 0$, the FD does not change with length scale and the system is self-similar, i.e., fractal. If Δs is small, then the system is closer to being fractal and the cells are more clustered.

Hotspot analysis. Another way to see if the cells are clustered or spread out is to determine the fraction of area where there are density 'hotspots', i.e., where the density of cells of a given type, e.g., $CD20^+$ B cells, is above average. To do this analysis, each $CD20^+$ B cell, say, is represented by a two-dimensional Gaussian distribution that represents the local density due to that cell. The width of the Gaussian is 2σ where σ^2 is the variance of the Gaussian. We then impose a square lattice of points (with lattice constant a) over the image and add the Gaussian weights at each lattice point (see figure 3(B)). The resulting sum is the local $CD20^+$ B cell density. We then average over the entire lattice of points to find the average density and calculate the fraction of lattice points greater than the average for that image. We refer to this as the fraction of the (image) area with hotspots. Note that this fraction is independent of the value of the average B cell density since the hotspots are measured relative to the average density in each particular image. We then average over images and vary σ. The larger the fraction of hotspots is, the more spread out the cells are.

Our hotspot analysis differs from the Getis–Ord hotspot analysis [83, 85] which requires dividing the image up into regions and depends on the cell counts in neighboring regions. Our hotspot method is completely local in the sense that the cell density at one grid point does not depend on the density at neighboring points.

In applying these techniques to the B cells and killer T cells in the tumors of 37 TNBC patients, we found that the FD difference and the area under the curve of hotspot fraction vs σ is larger for good outcome (see figure 4), indicating that these cells are more spread out in the cases where the tumor does not recur and more aggregated in cases where there is recurrence.

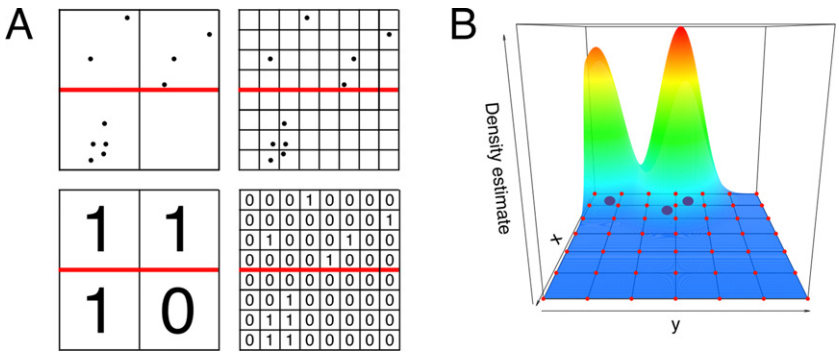

Figure 3. (A) Diagram illustrating how FD difference can distinguish the difference between spread out cells and clustered cells. The upper halves (above the red lines) of the two images show points that are spread out while the lower halves show clustered points. Both upper and lower halves have the same number of points. At long length scales (big boxes) the FD is 2 in the upper half but not in the lower half. At small length scales (small boxes), there is the same number of boxes with points and hence the same FD. The FD difference is greater in the upper half because the points are more spread out in the upper half. (B) Diagram illustrates hotspot analysis using the Gaussian method for density estimation. Three large blue points indicate the locations of three cells. Each cell's contribution to the local density is represented by a Gaussian distribution. The width of the Gaussian is 2σ. The two mountains over the three cells represent the superposition of their Gaussian weights, i.e., the local cell density. The small red points are the grid points where the local Gaussian weights are summed. Adapted with permission from [107]. © 2020 World Scientific Publishing Co Pte Ltd.

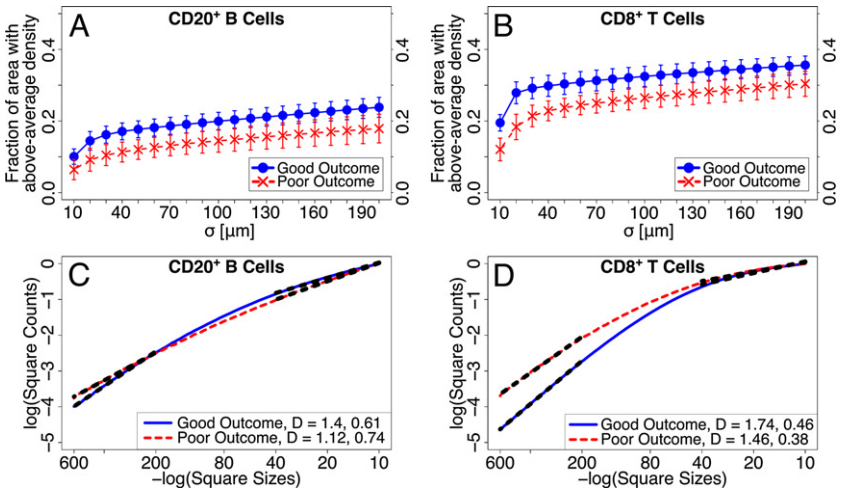

Figure 4. (A) and (B) Fraction of area with (A) $CD20^+$ B cell hotspots (B) $CD8^+$ T cell hotspots vs σ is greater for good outcome (blue) compared to poor outcome (red), indicating that the cells are more spatially dispersed in good outcome. The error bars correspond to 95% confidence intervals. (C) Log–log plot of the number of squares with at least one $CD20^+$ B cell vs the inverse box size. (Logarithms are base e.) At long length scales (200–600 microns on the left side of plot), the mean FD s (slope) is 1.4 for good outcome (blue) and 1.12 for poor outcome (red). The p-value for good vs poor outcome is 0.02 at long length scales. At short length scales (10–40 microns on the right side of the plot), the mean FD is 0.61 for good outcome and 0.74 for poor outcome. The p-value for good vs poor outcome is 0.1 at short length scales. The FD difference $\Delta s = 0.78$ for good outcome is greater than $\Delta s = 0.38$ for poor outcome. So B cells are more spread out for good outcome. The p-value associated with Δs is 9×10^{-5}. (D) Log–log plot of the number of squares with at least one $CD8^+$ T cell vs the inverse box size. At long length scales (200–600 microns on the left side of plot), the mean FD s (slope) is 1.74 for good outcome (blue) and 1.46 for poor outcome (red). The p-value for good vs poor outcome is 0.0005 at long length scales. At short length scales (10–40 microns on the right side of the plot), the mean FD is 0.46 for good outcome, 0.38 for poor outcome. The p-value for good vs poor outcome is 0.2 at short length scales. The FD difference $\Delta s = 1.28$ for good outcome is greater than $\Delta s = 1.08$ for poor outcome. So $CD8^+$ T cells are more spread out for good outcome. The p-value associated with Δs is 0.006. (C) and (D) Black dashed lines show the least squares linear regression fit at long and short length scales. Because different images had different overall areas, we normalized the number $n(L)$ of boxes with 1's by the total number $N(L)$ of boxes with cells in computing the FD; thus the y-axis values are negative.

Nearest neighbor (NN) distances between cells of a given type. An *a priori* obvious way to quantify how spread out the cells of a given type, e.g. B cells, are in an image would be to measure the mean or median NN distances between those cells. However, most B cells are quite close (5–20 μm) to another B cell, so the NN distance just reflects the (inverse of the) local cell density rather than the spatial dispersion at long length scales. However, if the B cells (or cells of a given type) are thinned, then the mean or median nearest neighbor distances can be a good measure of the spatial dispersion of cells [99].

3.6. A maximum entropy approach to quantifying the spatial distribution of immune cells

Entropy is a measure of disorder. The greater the number of configurations or the number of ways of arranging things, the

greater the entropy is. Mathematically, the entropy is the logarithm of the number of states or ways of arranging things. Since there can be millions of immune cells in an image of the tissue, the number of ways of arranging all these cells and hence, the associated entropy is enormous. To reduce the entropy to a manageable value, we took the following approach. We divided the image of the tissue into blocks of size $L \times L$. Each block or matrix was subdivided further into 3×3 squares like a tic-tac-toe board. As before, for each square, we then ask a binary (yes–no) question, e.g., 'is there at least one T cell in the square?' If the answer is yes, we assign a 1 to that square. If the answer is no, we assign a 0 to the square. There are a total of 2^9 or 512 possible states for a block of 3×3 squares. So the entropy for total randomness (all states equally likely) is $S_0 = \ln(512)$. We chose 3×3 matrices in order to obtain meaningful statistics, i.e., we wanted the total number of possible states to be much less than the number of samples (statistical trials). Let $P(x_i)$ be the probability of finding the ith configuration x_i where i varies from 1 to 512. Then the entropy is

$$S = -\sum_{i=1}^{512} P(x_i)\, \ln\left[P(x_i)\right]. \tag{7}$$

Maximum entropy. Maximum entropy is a widely used technique to find the probability $P(x_i)$ subject to the constraint that it produces the observed expectation values of various moments of the distribution [102, 103]. It is a minimalist approach that does not impose any other constraints or assumptions. Let us begin by considering $f_\mu(x_i)$ be the μth measureable quantity when the system is in the state x_i. The observed expectation value is $\langle f_\mu \rangle_{\text{expt}}$. The constraint is that the probability $P(x_i)$ satisfy

$$\sum_i P(x_i)\, f_\mu(x_i) = \langle f_\mu \rangle_{\text{expt}}. \tag{8}$$

To do this we maximize the entropy functional:

$$\tilde{S}\left[P(x)\right] = -\sum_i P(x_i) \ln P(x_i) - \sum_{\mu=1}^{K} \lambda_\mu \left[\sum_i P(x_i) f_\mu(x_i) - \langle f_\mu \rangle_{\text{expt}}\right], \tag{9}$$

where λ_μ are the Lagrange multipliers that are adjusted so that the constraints are satisfied. Maximizing $\tilde{S}$ yields the probability

$$P(x_i) = \frac{1}{Z} \exp\left[-\sum_{\mu=1}^{K} \lambda_\mu f_\mu(x_i)\right], \tag{10}$$

where Z is the normalization constant. The entropy is then given by

$$S = -\sum_i P(x_i) \ln\left[P(x_i)\right] \tag{11}$$

Note that if the energy of a physical system in state x is $E(x)$ and we only know the expectation value of the energy:

$$\langle E \rangle = \sum_x P(x)\, E(x) \tag{12}$$

then the maximum entropy distribution given by equation (10) becomes the Boltzmann distribution:

$$P(x) = \frac{1}{Z} \exp\left[-\lambda E(x)\right], \tag{13}$$

where the Lagrange multiplier $\lambda = 1/(k_B T)$ where k_B is Boltzmann's constant and T is temperature.

Moments of the distribution, probabilities and entropies [104]. The observables that set the constraints are the moments of the distribution. The zeroth moment is the normalization condition on the probability. In our case, the first moment is the average matrix occupancy $\langle p \rangle$, i.e., the average fraction of squares that have a '1' in a matrix of 3×3 squares. If the first order probability $P_1(x_i)$ is normalized and is subject to the constraint that it gives the observed value $\langle p \rangle_{\text{expt}}$ of the first moment, then this gives the first order entropy S_1:

$$S_1 = -\sum_{i=1}^{512} P_1(x_i) \ln\left[P_1(x_i)\right], \tag{14}$$

where

$$P_1(x) = \frac{1}{Z} \exp\left[-\lambda_1 p(x)\right] \tag{15}$$

and the Lagrange multiplier λ_1 is set by the constraint of the average occupancy $\langle p \rangle$:

$$(p)_{\text{expt}} = \sum_{i=1}^{512} P_1(x_i)\, p(x_i), \tag{16}$$

where $p(x_i)$ is the occupancy of the ith configuration x_i of the 3×3 matrix of 1's and 0's. The connected information of order 1 is defined by

$$I_1 = S_0 - S_1 \tag{17}$$

and tells us how much the occupancy or density reduces the entropy from the completely random case [104]. (Note that this definition of occupancy is slightly different from our earlier description where we placed a grid of squares covering the entire image of the tissue, and defined the occupancy to be the fraction of all the squares in grid with 1's.)

The second moment consists of the average occurrence rates of various patterns with two squares that have 1's. Ignoring translations, rotations and reflections, there are 5 types of such patterns in a matrix of 3×3 squares as shown in figure 5. If $P_2(x_i)$ is normalized and gives the observed value of $\langle p \rangle$ as well as those of the 2-square occurrence rates according to equations (8) and (9), then this gives the second order entropy S_2:

$$S_2 = -\sum_{i=1}^{512} P_2(x_i) \ln\left[P_2(x_i)\right]. \tag{18}$$

The connected information of order 2

$$I_2 = S_1 - S_2 \tag{19}$$

indicates how much the constraints of the second moment reduce the first order entropy. Similarly, the third moment corresponds to 10 different arrangements of 3 squares that have '1' in a 9-square matrix, ignoring translations, rotations and

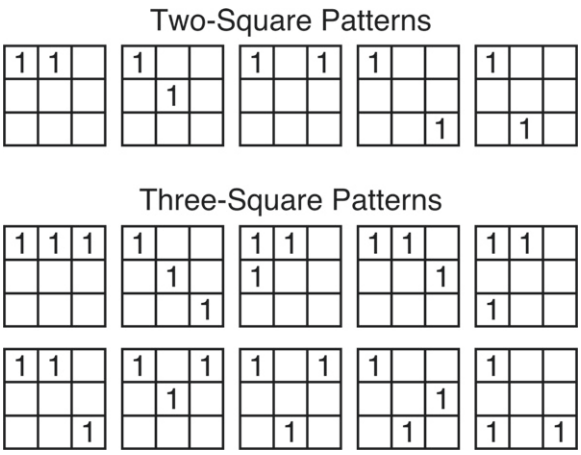

Figure 5. The five two-square and ten three-square patterns possible for a 3 × 3 matrix, ignoring translations, rotations, and reflections. The two-square (three-cell) pattern has two (three) 1's and the blank squares can be either 1 or 0. Each pattern corresponds to a state. Rotations, translations and reflections of a given pattern correspond to different states (out of 512 possible states) but are part of the same pattern. The fraction of times that a given pattern μ occurs equals $\langle f_\mu \rangle_{\text{expt}}$ in equations (8) and (9).

reflections as shown in figure 5. $P_3(x_i)$ gives the third order entropy S_3, and the connected information of order 3 is given by $I_3 = S_2 - S_3$. The multi-information is defined by

$$I_N = S_0 - S_N, \tag{20}$$

where the entropy S_N is given by using the actual histogram distribution $P_N(x_i)$ found from the data:

$$S_N = -\sum_{i=1}^{512} P_N(x_i) \ln [P_N(x_i)] \tag{21}$$

To obtain the behavior at different length scales, the size of the 3 × 3 matrices can be varied. While the first moment of the distribution gives the average occupancy, moments of order 2 and higher, along with the associated probabilities, entropies and connected informations, indicate the importance of spatial correlations at various length scales.

Relation of occupancy and I_1. We note that I_1 is related to occupancy in the following way for a 3 × 3 matrix of squares. Let the occupancy p be the probability that a square will have a '1'. Then $q = (1 - p)$ is the probability that a square will have a '0'. Let x_i denote a given state or arrangement of 1's and 0's in a 3 × 3 matrix. Then the probability of having a given state x_i with n 1's is given by $\tilde{P}_{n,p} = p^n q^{9-n}$. The first order entropy just depends on the occupancy and is given by

$$\begin{aligned} S_1 &= -\sum_{i=1}^{512} P_1(x_i) \ln [P_1(x_i)] \\ &= -\sum_{n=0}^{9} \left[\frac{9!}{n!\,(9-n)!} \right] \tilde{P}_{n,p} \ln \left[\tilde{P}_{n,p} \right], \end{aligned} \tag{22}$$

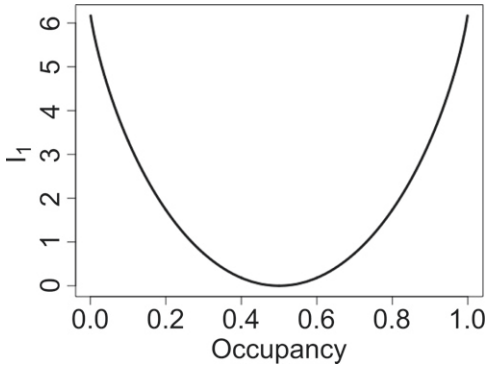

Figure 6. I_1 vs occupancy. When the occupancy = 0.5, the entropy $S_0 = S_1$, and I_1 is zero, resulting in a minimum in I_1 because that is where there is a 50% chance of having a 0 or a 1 in each square.

where we used the binomial coefficient to reduce the number of terms in the sum from 512 to 10 since the binomial coefficient gives the number of ways to arrange n 1's in a 3 × 3 matrix. Recall from equation (17) that the connected information $I_1 = S_0 - S_1$ where $S_0 = \ln(512) = 6.238$. Note that $I_1 = 0$ at $p = q = 0.5$ because $\tilde{P}_{n,p=0.5} = (1/2)^9 = 1/512$. We can explicitly evaluate equation (22) and compute I_1 versus occupancy. This is plotted in figure 6. Notice that for occupancy $p > 0.5$, the greater the occupancy, the higher I_1 is, whereas for $p < 0.5$, the greater the occupancy, the lower I_1 is.

Kullback–Leibler divergence. Connected information, e.g., I_1 and I_2, provides one way to compare probability distributions. Another way to compare different probability distributions, e.g., P_A and P_B, is through the Kullback–Leibler (KL) divergence (or relative entropy) [105, 106]:

$$D_{AB} = -\sum_i P_A(x_i) \ln \left(\frac{P_B(x_i)}{P_A(x_i)} \right). \tag{23}$$

This is a measure of how different a probability distribution P_B is from a reference (*a priori*) probability distribution P_A. If the distributions are identical, then $D_{AB} = 0$; otherwise D_{AB} is always positive.

4. Application of maximum entropy to breast cancer

4.1. Triple negative breast cancer patient cohort

We have used our maximum entropy approach to analyze the spatial distribution of various types of TILs in 2D images of TILs in immunohistochemistry-based images of primary tumor tissue from 37 patients with TNBC prior to any treatment. In this study, we defined patients with no recurrence within 5 years after surgery as good clinical outcome ($n = 24$) and patients who had recurrence within 3 years after surgery as poor clinical outcome ($n = 13$). All the patients were subsequently treated with standard chemotherapy; some also had radiotherapy.

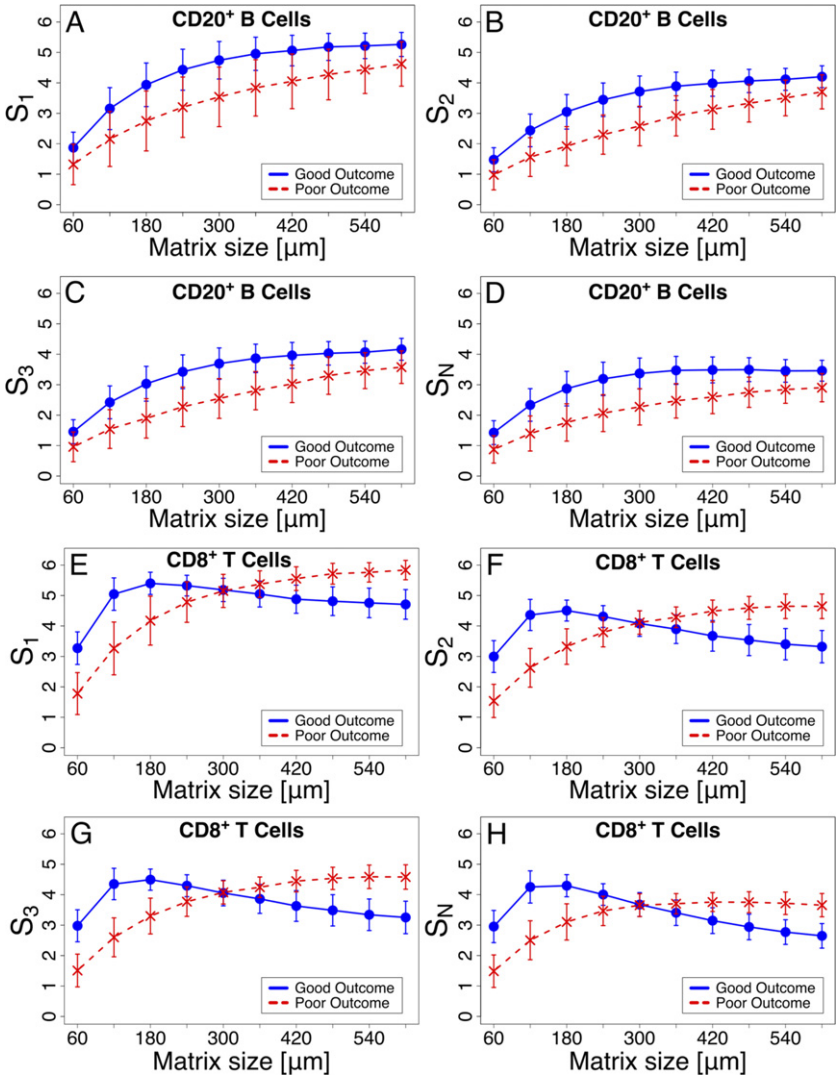

Figure 7. Entropies S_1, S_2, S_3 and S_N vs matrix size for (A)–(D) $CD20^+$ B cells and (E)–(H) $CD8^+$T cells. Blue solid lines are for good outcome and red dashed lines are for poor outcome. The higher order entropies look similar to S_1 because they are dominated by S_1. The error bars represent 95% confidence intervals. (A) S_1 (B) S_2 (C) S_3 (D) S_N (E) S_1 (F) S_2 (G) S_3 (H) S_N.

4.2. Preparation of images: multispectral staining of different cell types

To analyze the spatial distribution of various types of TILs, we first identified the locations of cells in 2D images of archived formalin fixed paraffin embedded (FFPE) tumor tissues from 37 TNBC patients. Each cell type was immunostained and labeled with a different color chromophore. This means that the tissue is treated with an antibody that binds to a protein that is specific to a certain cell type. For example, the protein CD3 is expressed on all types of T cells but not on B cells. So if we attach a green colored molecule or chromophore to CD3 antibodies, then T cells that bind the antibodies will appear green. Each image was restricted to tumor-associated regions and excluded necrotic and fibrotic areas determined by a pathologist. (Necrotic tissue consists of dead cells. Fibrotic tissue has excess fibrous connective tissue, e.g., scar tissue.) More details about our methods can be found in Wortman *et al* [107].

5. Results

5.1. Entropies vs length scale

In figure 7, we plot the entropies S_1, S_2, S_3 and S_N versus matrix size for good and poor outcome for B cells and cytotoxic $CD8^+$ T cells. (Recall that a matrix has 3×3 squares.) Notice that there is a distinct difference between good and poor outcome, though the shape of the curves for B cells is similar because the densities of B cells, which affect the entropies, are comparable between good (3.0×10^2 mm^{-2}) and poor (2.3×10^2 mm^{-2}) outcome. If we integrate under the curves to get the AUC, then good outcome has a larger AUC for B cells compared to poor outcome. For example, the B-cell AUC for S_N is 31 for good outcome compared to 22 for poor outcome. This difference is significant (p-value $= 0.01$) and reflects the fact that the B cells are more spread out for good outcome and more aggregated for poor outcome.

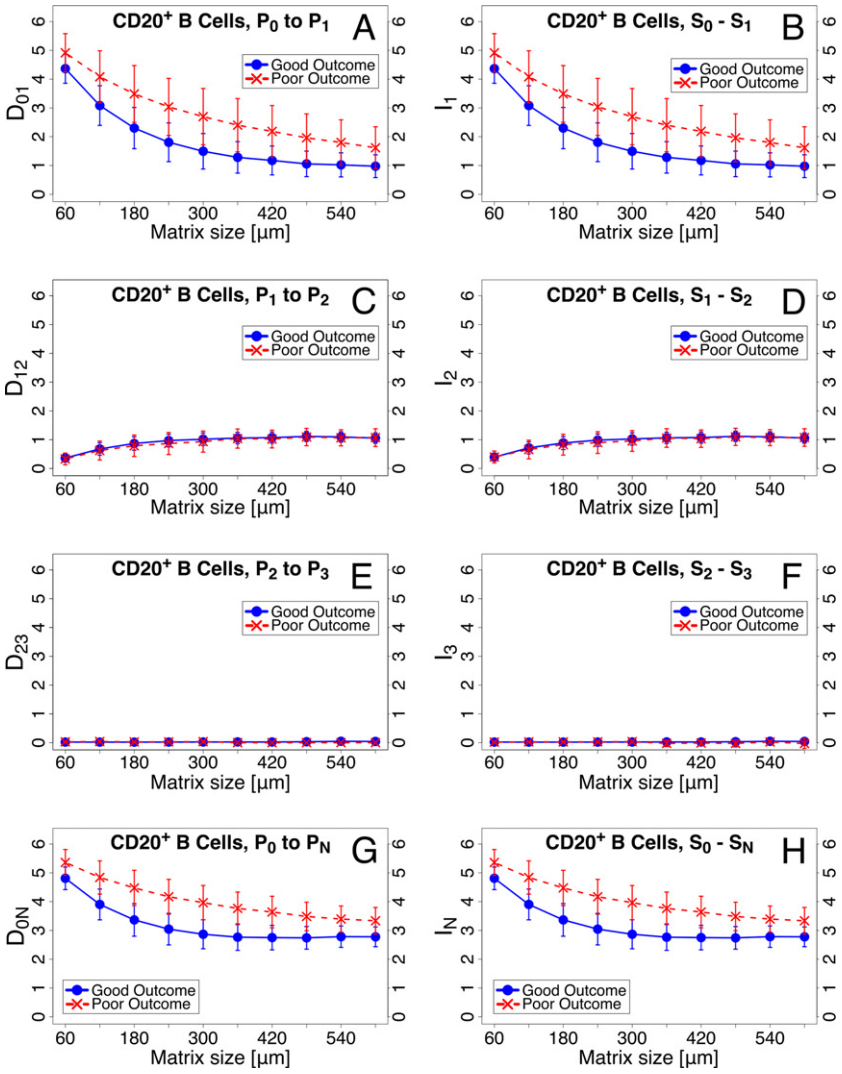

Figure 8. Information moments and Kullback–Leibler divergences vs matrix size for CD20$^+$ B cells. Blue solid lines are for good outcome and red dashed lines are for poor outcome. The error bars represent 95% confidence intervals. (A) D_{01} (B) I_1 (C) D_{12} (D) I_2 (E) D_{23} (F) I_3 (G) D_{0N} (H) I_N.

However, there is no significant difference between the good and poor outcome AUC for killer CD8$^+$ T cells because the curves cross. The difference between good and poor outcome in the shape of the curves for CD8$^+$ T cells is due to the significant difference in densities by about a factor of two between good (4.5×10^4 cells mm^{-2}) and poor (2.1×10^4 cells mm^{-2}) outcome. The maximum in S_1 vs matrix size for good outcome occurs at the matrix size where the probability p of having at least one CD8$^+$ T cell in a square is closest to 0.5. Recall that the case of $p = q = 0.5$ gives the largest value of the entropy S_0. Since good outcome has a higher CD8$^+$ T cell density, the entropy curves reach a maximum at a smaller matrix size compared to poor outcome.

Notice that for a given cell type and outcome, the entropy curves in figure 7 are similar to those for S_1. This is because S_1 dominates the entropy. This is clearly seen in figures 8 and 9 where the connected information moments (I_1, I_2, I_3, and I_N) and KL divergences (D_{01}, D_{12}, D_{23}, and D_{0N}) are plotted for B cells and CD8$^+$ T cells. One can see that similar information is conveyed for the pairs (I_1 and D_{01}), (I_2 and D_{12}), etc. Both connected information moments and KL divergences are ways to compare two distributions. I_1 and D_{01} differ between good and poor outcome but there is no noticeable dependence on outcome for I_2, I_3, D_{12}, and D_{23}. In fact, I_3 and D_{23} are negligible. I_2 and D_{12} are nonzero, indicating that $S_1 \neq S_2$ and hence, that $P_1 \neq P_2$. This reflects spatial correlations resulting from clustering of the cells since the cells need to be in the same matrix to produce the two square patterns shown in figure 5. The lack of any difference between good and poor outcome for I_2, I_3, D_{12}, and D_{23} implies that the difference in spatial correlations of the cells is not clinically significant. I_N is similar to I_1 because it is dominated by I_1, and D_{0N} is similar to and dominated by D_{01}. The fact that the difference between good and poor outcomes is only noticeable for the first moment (I_1 and D_{01}) is why we focused on quantities described earlier like occupancy, FDs, and fraction of area with density hotspots.

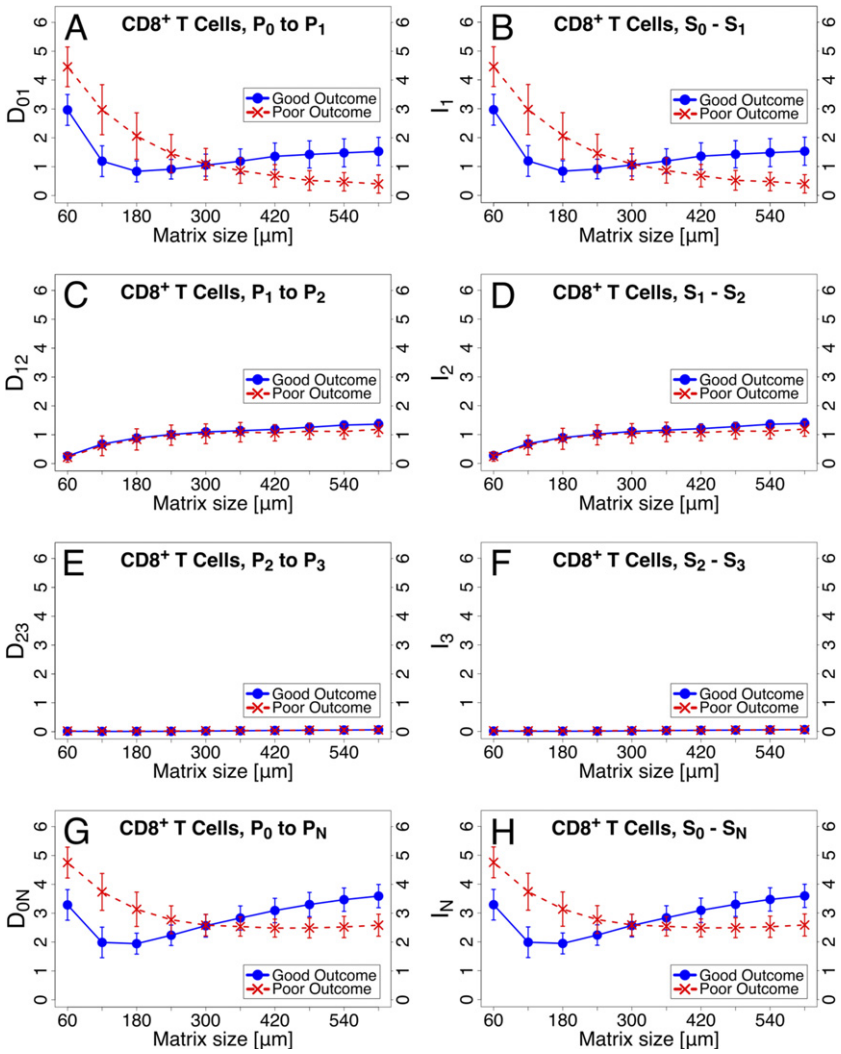

Figure 9. Information moments and KL divergences vs matrix size for $CD8^+$ T cells. Blue solid lines are for good outcome and red dashed lines are for poor outcome. The error bars represent 95% confidence intervals. (A) D_{01} (B) I_1 (C) D_{12} (D) I_2 (E) D_{23} (F) I_3 (G) D_{0N} (H) I_N.

6. Discussion

We have seen that going beyond the density of immune cells, e.g., B cells or T cells, and looking at their spatial distribution in tumors can reveal differences associated with clinical outcome, i.e., whether or not cancer recurs. We have developed techniques to quantify the spatial distribution of cancer and immune cells over a range of length scales. Occupancy, FD difference and the fraction of area with density hotspots are useful for determining to what degree cells are spread out or aggregated. In our maximum entropy approach, S_1, I_1 and D_{01} reflect information contained in the first moments of the distribution and are sensitive to the density of cells while higher moments, e.g., S_2, I_2 and D_{12}, are a way to ascertain the spatial correlation of cells on different length scales, though we do not see any clinically significant difference in the spatial correlations of B and cytotoxic $CD8^+$ T cells.

Our findings raise a number of important questions about the spatial distribution of TILs. First, what determines the spatial distribution of TILs? Certainly, chemical signals, i.e., cytokines and chemokines help to dictate where immune cells go. In addition, we speculate that the somewhat fractal spatial distribution of TILs may arise from the branching trajectories of the B and T cells as they patrol the tissue. Branching structures such as trees and plant roots are self-similar, and hence fractal, because they look the same over a range of length scales, i.e., over a range of magnifications. It may be that the paths that B and T cells travel along have a branching structure because these cells have to go around physical obstacles such as other cells, blood vessels, and collagen fibers. In addition, T cells are known to follow along the outside of blood vessels and collagen fibers [108, 109] which can have a branching architecture.

Second, what are the roles of the B and T cells in the tumor? Cytotoxic T cells are presumably able to identify neoantigens on cancer cells and kill those cells, but what are the B cells doing in the tumor? As we mentioned earlier, B cells are best known for producing antibodies but they can also perform other functions such as presenting antigens for (helper) T cells to inspect and secreting cytokines which are chemical signaling molecules that direct the actions of other immune cells. The $CD20^+$ B cells that we studied are not antibody

producing plasma cells since plasma cells do not express CD20. So they may be acting as APCs and/or secreting cytokines.

Third, why do the spatial distributions of B and T cells differ between good and poor clinical outcome? In particular, one could also ask why B and T cells are more spread out for good clinical outcome as found in references [99, 107]. One possibility is that the difference in spatial distribution reflects differences in the spatial topography (obstacles) of the stroma in the TME. However, in FFPE tissue sections, we performed immunohistochemical staining of collagen *I* which did not yield differences in the spatial distribution of collagen *I* between good and poor outcome (data not shown). This indicates that differences in physical topography may not be the explanation. Furthermore, there are indications that collagen fibers around cancer cell islands do not present a barrier to T cells [110]. In addition, we find that the spatial distribution of cells in the stroma (which is where most immune cells reside) cannot explain the clinical difference in the spatial distribution of TILs [107].

The tendency of lymphocytes to aggregate in poor outcome suggests a lack of motility, e.g., in overcoming physical barriers in the stroma such as collagen fibers. This may be due to a lack of chemokine signaling and cognate antigens, or a lack of oxygen and nutrients due to poorly organized leaky vasculature that produces hypoxic regions, or poor metabolism resulting from dysfunctional mitochondria [111]. (Mitochondria are the power plants of the cell; they produce ATP which fuels cellular processes.)

In good outcome, it may be that lymphocytes are better at immune surveillance when they are more spread out. For example, antigen-presenting B cells may be more likely to acquire and successfully present cancer neo-antigens to helper T cells if they are able to interact with both cancer cells and other immune cells by spreading out. Widely dispersed B and T cells in good outcome patients should be more successful in finding their cognate (matching) antigens within the TME. In addition, cytokine secreting B and T cells may cover a larger area with signaling molecules and may be better positioned to respond to chemokines. In any event, an even spatial distribution is a more effective strategy for B and T cell surveillance than sequestration in small parts of the tumor.

In inflamed tissues, including tumors, there are often large densely packed cellular clusters that have B and T cells segregated in a way reminiscent of lymph nodes. These organized lymphoid aggregates are known as tertiary lymphoid structures (TLS) and finding them in tumors is associated with a good prognosis [112]. Recent studies indicate that B cells in tumors, especially in conjunction with TLS, are significant predictors of a good response to immunotherapy, i.e., immune checkpoint inhibitors, in melanoma [69, 70], soft tissue sarcomas [71], and renal cell carcinoma (kidney cancer) [70]. However, we find that most B cells in tumors do not reside in TLS. Given that TLS with high lymphocyte density are linked to good prognosis, it is somewhat ironic that we find good outcome is associated with spatially dispersed B cells, which connotes low local concentrations of B cells and are the antithesis of regions of high density B cells (germinal centers) found in mature TLS.

Fourth, it is rather odd *prima facie* that we are able to give a prognosis with any degree of accuracy based on tumor tissue that has been removed from a patient. The cells in the surgically removed tissue are no longer in the patient, yet their spatial distribution can be used to predict whether or not the cancer will recur in the next 3–5 years with an accuracy of 60%–80%. The reason for this is not understood. It may be that spatially dispersed B and T cells are associated with more immune engagement and the production of more memory B and T cells, leading to a better long-term outcome.

The statistical techniques that we have developed to quantify spatial distributions are novel. Unlike previous efforts to analyze spatial distributions at a single length scale, we have examined how the spatial distribution varies with length scale and how that can shed light on whether the cells are clustered or spread out spatially. On a more general level, these approaches are flexible and can be applied to a broad spectrum of problems. There are straightforward extensions of these approaches, e.g., to quantify the spatial distributions of various kinds of cells in metastatic tumors or to ascertain which patients are good candidates for various therapeutic treatments. However, one can go beyond simply the spatial distribution of cells or discrete entities. In determining the occupancy, FD and the difference in FDs, we laid down a grid of squares and asked a binary yes–no question of each square. In this paper, we asked questions like 'is there at least one $CD20^+$ B cell in this square?' However, in other contexts, one may be interested in other questions such as that of co-localization. For example, one could ask 'does the square have at least one T cell that is within 50 microns of a dendritic cell?' or 'does the square have at least one B cell and one T cell within 25 microns of a blood vessel?' Furthermore, these approaches could be applied to image analysis outside of biology, e.g., the distribution of galaxies in astrophysics.

In conclusion, we have presented novel techniques to quantify the spatial distribution of point-like objects. In applying these techniques to B and cytotoxic T cells in tumors, we found that the spatial arrangement of these immune cells is strongly correlated with clinical outcome, i.e., breast cancer recurrence. This highlights the importance of these immune cells in cancer and raises new questions about their role in preventing cancer.

Acknowledgments

We thank Dr. Ching Ouyang for helpful discussions. CCY thanks Dr. Arnold Levine and Dr. Larry Norton for helpful discussions. This work was supported by Stand Up To Cancer, The V Foundation, and the Breast Cancer Research Foundation. The work of CCY and JCW was also supported in part by the Cure Breast Cancer Foundation. The work of CCY was performed in part at the Aspen Center for Physics, which is supported by National Science Foundation Grant No. PHY-1607611.

ORCID iDs

Clare C Yu https://orcid.org/0000-0002-6565-2988
Travis Y Tu https://orcid.org/0000-0002-8167-313X

References

[1] 2019 All cancers fact sheet (source: GLOBOCAN 2018) available from: https://gco.iarc.fr/today/data/factsheets/cancers/39-All-cancers-fact-sheet.pdf
[2] Howlader N *et al* (ed) 2016 SEER cancer statistics review, 1975–2013, National Cancer Institute. Bethesda, MD [based on November 2015 SEER data submission, posted to the SEER web site, April 2016; available from: https://seer.cancer.gov/csr/1975_2013/
[3] Mukherjee S 2010 *The Emperor of All Maladies: A Biography of Cancer* (New York, NY: Scribner)
[4] Busch S *et al* 2012 Measurements of T_1-relaxation in *ex vivo* prostate tissue at 132 μT *Magn. Reson. Med.* **67** 1138–45
[5] Phan D T T *et al* 2017 A vascularized and perfused organ-on-a-chip platform for large-scale drug screening applications *Lab Chip* **17** 511–20
[6] Zhang Q, Lambert G, Liao D, Kim H, Robin K, Tung C-K, Pourmand N and Austin R H 2011 Acceleration of emergence of bacterial antibiotic resistance in connected microenvironments *Science* **333** 1764–7
[7] Wu A, Loutherback K, Lambert G, Estevez-Salmeron L, Tlsty T D, Austin R H and Sturm J C 2013 Cell motility and drug gradients in the emergence of resistance to chemotherapy *Proc. Natl Acad. Sci.* **110** 16103–8
[8] Luria S E and Delbruck M 1943 Mutations of bacteria from virus sensitivity to virus resistance *Genetics* **28** 491–511
[9] Norton L, Simon R, Brereton H D and Bogden A E 1976 Predicting the course of gompertzian growth *Nature* **264** 542–5
[10] Norton L and Simon R 1977 Tumor size, sensitivity to therapy, and design of treatment schedules *Cancer Treat. Rep.* **61** 1307–17
[11] Norton L and Simon R 1986 The Norton–Simon hypothesis revisited *Cancer Treat. Rep.* **70** 163–9
[12] Citron M L *et al* 2003 Randomized trial of dose-dense versus conventionally scheduled and sequential versus concurrent combination chemotherapy as postoperative adjuvant treatment of node-positive primary breast cancer: first report of intergroup trial C9741/cancer and Leukemia group B trial 9741 *J. Clin. Oncol.* **21** 1431–9
[13] Norton L 2005 Conceptual and practical implications of breast tissue geometry: toward a more effective, less toxic therapy *Oncol.* **10** 370–81
[14] Simon R and Norton L 2006 The Norton–Simon hypothesis: designing more effective and less toxic chemotherapeutic regimens *Nat. Rev. Clin. Oncol.* **3** 406–7
[15] Michor F and Beal K 2015 Improving cancer treatment via mathematical modeling: surmounting the challenges is worth the effort *Cell* **163** 1059–63
[16] Michor F, Liphardt J, Ferrari M and Widom J 2011 What does physics have to do with cancer? *Nat. Rev. Cancer* **11** 657–70
[17] Wodarz D and Komarova N L 2014 *Dynamics of Cancer: Mathematical Foundations of Oncology* (Singapore: World Scientific)
[18] Zheng Y, Sun Y, Torga G, Pienta K and Austin R 2020 Game theory cancer models of cancer cell-stromal cell dynamics using interacting particle systems *Biophys. Rev. Lett.* **15** 171–93
[19] Archetti M and Pienta K J 2019 Cooperation among cancer cells: applying game theory to cancer *Nat. Rev. Cancer* **19** 110–7
[20] Zhang J *et al* 2017 Integrating evolutionary dynamics into treatment of metastatic castrate-resistant prostate cancer *Nat. Commun.* **8** 1816
[21] Stanková K, Brown J S, Dalton W S and Gatenby R A 2019 Optimizing cancer treatment using game theory *JAMA Oncol.* **5** 96–103
[22] Butcher D T, Alliston T and Weaver V M 2009 A tense situation: forcing tumour progression *Nat. Rev. Cancer* **9** 108–22
[23] Mariappan Y K, Glaser K J and Ehman R L 2010 Magnetic resonance elastography: a review *Clin. Anat.* **23** 497–511
[24] Hansma P *et al* 2009 The tissue diagnostic instrument *Rev. Sci. Instrum.* **80** 054303
[25] Lopez J I, Kang I, You W-K, McDonald D M and Weaver V M 2011 In situforce mapping of mammary gland transformation *Int. Biol.* **3** 910–21
[26] Wang N and Ingber D E 1994 Control of cytoskeletal mechanics by extracellular matrix, cell shape, and mechanical tension *Biophys. J.* **66** 2181–9
[27] Bausch A R, Ziemann F, Boulbitch A A, Jacobson K and Sackmann E 1998 Local measurements of viscoelastic parameters of adherent cell surfaces by magnetic bead microrheometry *Biophys. J.* **75** 2038–49
[28] Mills J P *et al* 2004 Nonlinear elastic and viscoelastic deformation of the human red blood cell with optical tweezers *Mech. Chem. Biosyst.* **1** 169–80
[29] Brunner C, Niendorf A and Käs J A 2009 Passive and active single-cell biomechanics: a new perspective in cancer diagnosis *Soft Matter* **5** 2171–8
[30] Radmacher M, Fritz M, Kacher C M, Cleveland J P and Hansma P K 1996 Measuring the viscoelastic properties of human platelets with the atomic force microscope *Biophys. J.* **70** 556–67
[31] Remmerbach T W, Wottawah F, Dietrich J, Lincoln B, Wittekind C and Guck J 2009 Oral cancer diagnosis by mechanical phenotyping *Cancer Res.* **69** 1728–32
[32] Riching K M *et al* 2014 3D collagen alignment limits protrusions to enhance breast cancer cell persistence *Biophys. J.* **107** 2546–58
[33] Bi D, Lopez J H, Schwarz J M and Manning M L 2015 A density-independent rigidity transition in biological tissues *Nat. Phys.* **11** 1074
[34] Bi D P *et al* 2016 Motility-driven glass and jamming transitions in biological tissues *Phys. Rev.* X **6** 021011
[35] Park J-A *et al* 2015 Unjamming and cell shape in the asthmatic airway epithelium *Nat. Mater* **14** 1040–8
[36] Ferrari M 2010 Frontiers in cancer nanomedicine: directing mass transport through biological barriers *Trends Biotechnol.* **28** 181–8
[37] Begley C G and Ellis L M 2012 Raise standards for preclinical cancer research *Nature* **483** 531–3
[38] Prinz F, Schlange T and Asadullah K 2011 Believe it or not: how much can we rely on published data on potential drug targets? *Nat. Rev. Drug Discov.* **10** 712
[39] Kaiser J 2017 Are preprints the future of biology? A survival guide for scientists *Science* https://doi.org/10.1126/science.aaq0747
[40] Amend S R *et al* 2019 Polyploid giant cancer cells: unrecognized actuators of tumorigenesis, metastasis, and resistance *Prostate* **79** 1489–97
[41] Jain R K 2008 Taming vessels to treat cancer *Sci. Am.* **298** 56–63
[42] Jain R K 2014 Antiangiogenesis strategies revisited: from starving tumors to alleviating hypoxia *Cancer Cell* **26** 605–22
[43] Austin R 2017 Cancer biology still needs physicists *Nature* **550** 431
[44] Bray F, Ferlay J, Soerjomataram I, Siegel R L, Torre L A and Jemal A 2018 Global cancer statistics 2018: GLOBO-

CAN estimates of incidence and mortality worldwide for 36 cancers in 185 countries *CA: Cancer J. Clin.* **68** 394–424
[45] Siegel R L, Miller K D and Jemal A 2020 Cancer statistics, 2020 *Ca–Cancer J. Clin.* **70** 7–30
[46] Bae M S, Moon H-G, Han W, Noh D-Y, Ryu H S, Park I-A, Chang J M, Cho N and Moon W K 2016 Early stage triple-negative breast cancer: imaging and clinical-pathologic factors associated with recurrence *Radiology* **278** 356–64
[47] Siemann D W (ed) 2011 *Tumor Microenvironment* (New York: Wiley)
[48] Bissell M J and Hines W C 2011 Why don't we get more cancer? A proposed role of the microenvironment in restraining cancer progression *Nat. Med.* **17** 320–9
[49] Dolberg D, Hollingsworth R, Hertle M and Bissell M 1985 Wounding and its role in RSV-mediated tumor formation *Science* **230** 676–8
[50] Barcellos-Hoff M H and Ravani S A 2000 Irradiated mammary gland stroma promotes the expression of tumorigenic potential by unirradiated epithelial cells *Cancer Res.* **60** 1254–60
[51] Mintz B and Illmensee K 1975 Normal genetically mosaic mice produced from malignant teratocarcinoma cells *Proc. Natl Acad. Sci.* **72** 3585–9
[52] Sieweke M, Thompson N, Sporn M and Bissell M 1990 Mediation of wound-related Rous sarcoma virus tumorigenesis by TGF-beta *Science* **248** 1656–60
[53] Krall J A *et al* 2018 The systemic response to surgery triggers the outgrowth of distant immune-controlled tumors in mouse models of dormancy *Sci. Trans. Med.* **10** 3464
[54] Sompayrac L 2019 *How the Immune System Works* vol 158 6th edn Wiley) (Chichester)
[55] Lawrence M S *et al* 2013 Mutational heterogeneity in cancer and the search for new cancer-associated genes *Nature* **499** 214–8
[56] García-Aranda M and Redondo M 2019 Immunotherapy: a challenge of breast cancer treatment *Cancers* **11** 121822
[57] Immunomodulators available from: https://cancerresearch.org/immunotherapy/treatment-types/immunomodulators-checkpoint-inhibitors
[58] García-Aranda M and Redondo M 2019 Targeting protein kinases to enhance the response to anti-PD-1/PD-L1 immunotherapy *Int. J. Mol. Sci.* **20** 092296
[59] Ayoub N M, Al-Shami K M and Yaghan R J 2019 Immunotherapy for HER2-positive breast cancer: recent advances and combination therapeutic *Breast Cancer: Targets Ther.* **11** 53–69
[60] Helwick C 2020 (Harborside Press) *The ASCO Post* USA April 10, 2020 https://ascopost.com/issues/april-10-2020/immunotherapy-comes-of-age-in-breast-cancer/
[61] Savas P, Salgado R, Denkert C, Sotiriou C, Darcy P K, Smyth M J and Loi S 2016 Clinical relevance of host immunity in breast cancer: from TILs to the clinic *Nat. Rev. Clin. Oncol.* **13** 228–41
[62] Schmid P *et al* 2018 Atezolizumab and nab-paclitaxel in advanced triple-negative breast cancer *New Engl. J. Med.* **379** 2108–21
[63] SM O B and Mathis J M 2018 Oncolytic virotherapy for breast cancer treatment *Curr. Gene Ther.* **18** 192–205
[64] Criscitiello C, Viale G and Curigliano G 2019 Peptide vaccines in early breast cancer *Breast* **44** 128–34
[65] Castle J C *et al* 2019 Mutation-derived neoantigens for cancer immunotherapy *Front. Immunol.* **10** 1856
[66] Toraya-Brown S and Fiering S 2014 Local tumour hyperthermia as immunotherapy for metastatic cancer *Int. J. Hyperth.* **30** 531–9
[67] Skitzki J J, Repasky E A and Evans S S 2009 Hyperthermia as an immunotherapy strategy for cancer *Curr. Opin. Invest. Drugs* **10** 550–8
[68] Uryvaev A *et al* 2018 The role of tumor-infiltrating lymphocytes (TILs) as a predictive biomarker of response to anti-PD1 therapy in patients with metastatic non-small cell lung cancer or metastatic melanoma *Med. Oncol.* **35** 25
[69] Cabrita R *et al* 2020 Tertiary lymphoid structures improve immunotherapy and survival in melanoma *Nature* **577** 561–5
[70] Helmink B A *et al* 2020 B cells and tertiary lymphoid structures promote immunotherapy response *Nature* **577** 549–55
[71] Petitprez F *et al* 2020 B cells are associated with survival and immunotherapy response in sarcoma *Nature* **577** 556–60
[72] Fridman W H, Pagès F, Sautès-Fridman C and Galon J 2012 The immune contexture in human tumours: impact on clinical outcome *Nat. Rev. Cancer* **12** 298–306
[73] Mlecnik B *et al* 2011 Histopathologic-based prognostic factors of colorectal cancers are associated with the state of the local immune reaction *J. Clin. Oncol.* **29** 610–8
[74] Angell H and Galon J 2013 From the immune contexture to the Immunoscore: the role of prognostic and predictive immune markers in cancer *Curr. Opin. Immunol.* **25** 261–7
[75] Galon J 2006 Type, density, and location of immune cells within human colorectal tumors predict clinical outcome *Science* **313** 1960–4
[76] Shen M, Wang J and Ren X 2018 New insights into tumor-infiltrating B lymphocytes in breast cancer: clinical impacts and regulatory mechanisms *Front. Immunol.* **9** 470
[77] Tsou P, Katayama H, Ostrin E J and Hanash S M 2016 The emerging role of B cells in tumor immunity *Cancer Res.* **76** 5597–601
[78] Berthel A, Zoernig I, Valous N A, Kahlert C, Klupp F, Ulrich A, Weitz J, Jaeger D and Halama N 2017 Detailed resolution analysis reveals spatial T cell heterogeneity in the invasive margin of colorectal cancer liver metastases associated with improved survival *Oncoimmunology* **6** e1286436
[79] Saltz J *et al* 2018 Spatial organization and molecular correlation of tumor-infiltrating lymphocytes using deep learning on pathology images *Cell Rep.* **23** 181–93
[80] Kather J N *et al* 2018 Topography of cancer-associated immune cells in human solid tumors *Elife* **7** 36967
[81] Gillies R J, Verduzco D and Gatenby R A 2012 Evolutionary dynamics of carcinogenesis and why targeted therapy does not work *Nat. Rev. Cancer* **12** 487–93
[82] Junttila M R and de Sauvage F J 2013 Influence of tumour micro-environment heterogeneity on therapeutic response *Nature* **501** 346–54
[83] Yuan Y 2016 Spatial heterogeneity in the tumor microenvironment *Cold Spring Harbor Perspect. Med.* **6** 1–18
[84] Maley C C *et al* 2015 An ecological measure of immune-cancer colocalization as a prognostic factor for breast cancer *Breast Cancer Res.* **17** 131
[85] Getis A and Ord J K 1992 The analysis of spatial association by use of distance statistics *Geogr. Anal.* **24** 189–206
[86] Nawaz S, Heindl A, Koelble K and Yuan Y 2015 Beyond immune density: critical role of spatial heterogeneity in estrogen receptor-negative breast cancer *Mod. Pathol.* **28** 766–77
[87] Yuan Y 2015 Modelling the spatial heterogeneity and molecular correlates of lymphocytic infiltration in triple-negative breast cancer *J. R. Soc. Interface* **12** 1153
[88] Natrajan R, Sailem H, Mardakheh F K, Arias Garcia M, Tape C J, Dowsett M, Bakal C and Yuan Y 2016 Microenvironmental heterogeneity parallels breast cancer progression: a histology-genomic integration analysis *PLoS Med.* **13** e1001961
[89] Mandelbrot B B 1983 *The Fractal Geometry of Nature* (New York: W H Freeman and Co) p 468
[90] Tambasco M, Eliasziw M and Magliocco A M 2010 Morphologic complexity of epithelial architecture for predicting invasive breast cancer survival *J. Trans. Med.* **8** 140

[91] Velanovich V 1998 Fractal analysis of mammographic lesions: a prospective, blinded trial *Breast Cancer Res. Treat.* **49** 245–9
[92] Chan A and Tuszynski J A 2016 Automatic prediction of tumour malignancy in breast cancer with fractal dimension *R. Soc. Open Sci.* **3** 160558
[93] Baish J W and Jain R K 1998 Cancer, angiogenesis and fractals *Nat. Med.* **4** 984
[94] Baish J W and Jain R K 2000 Fractals and cancer *Cancer Res.* **60** 3683–8
[95] Lennon F E *et al* 2016 Unique fractal evaluation and therapeutic implications of mitochondrial morphology in malignant mesothelioma *Sci. Rep.* **6** 24578
[96] Bose P *et al* 2015 Fractal analysis of nuclear histology integrates tumor and stromal features into a single prognostic factor of the oral cancer microenvironment *BMC Cancer* **15** 409
[97] Waliszewski P, Wagenlehner F, Gattenlöhner S and Weidner W 2015 On the relationship between tumor structure and complexity of the spatial distribution of cancer cell nuclei: a fractal geometrical model of prostate carcinoma *Prostate* **75** 399–414
[98] Waliszewski P 2016 The quantitative criteria based on the fractal dimensions, entropy, and lacunarity for the spatial distribution of cancer cell nuclei enable identification of low or high aggressive prostate carcinomas *Front. Physiol.* **7** 34
[99] Wortman J C *et al* 2019 Fractal dimension, occupancy and hotspot analyses of B cell spatial distribution predict clinical outcome in breast cancer https://doi.org/10.1101/678607
[100] Zar J H 2010 *Biostatistical Analysis* (Upper Saddle River, NJ: Pearson Prentice Hall)
[101] Peitgen H-O, Jürgens H and Saupe D 1992 *Chaos and Fractals: New Frontiers of Science* (New York: Springer)
[102] Bialek W 2012 *Searching for Principles* (Princeton, NJ: Princeton University Press)
[103] Jaynes E T 1957 Information theory and statistical mechanics *Phys. Rev.* **106** 620–30
[104] Schneidman E *et al* 2003 Network information and connected correlations *Phys. Rev. Lett.* **91** 238701
[105] Kullback S and Leibler R A 1951 On information and sufficiency *Ann. Math. Stat.* **22** 79–86
[106] Kullback S 1959 *Information Theory and Statistics* (New York: Dover)
[107] Wortman J C *et al* 2020 Occupancy and fractal dimension analyses of the spatial distribution of cytotoxic ($CD8^+$) T cells infiltrating the tumor microenvironment in triple negative breast cancer *Biophys. Rev. Lett.* **15** 83–98
[108] Boissonnas A, Fetler L, Zeelenberg I S, Hugues S and Amigorena S 2007 *In vivo* imaging of cytotoxic T cell infiltration and elimination of a solid tumor *J. Exp. Med.* **204** 345–56
[109] Kuczek D E *et al* 2019 Collagen density regulates the activity of tumor-infiltrating T cells *J. Immunother. Cancer* **7** 68
[110] Li X, Gruosso T, Zuo D, Omeroglu A, Meterissian S, Guiot M-C, Salazar A, Park M and Levine H 2019 Infiltration of $CD8^+$ T cells into tumor cell clusters in triple-negative breast cancer *Proc. Natl Acad. Sci. USA* **116** 3678–87
[111] Yu Y R *et al* 2020 Disturbed mitochondrial dynamics in $CD8(^+)$ TILs reinforce T cell exhaustion **21** 1540–51 *Nat. Immunol.*
[112] Sautès-Fridman C, Petitprez F, Calderaro J and Fridman W H 2019 Tertiary lymphoid structures in the era of cancer immunotherapy *Nat. Rev. Cancer* **19** 307–25

Clare Yu is a Professor of Physics and Astronomy at the University of California, Irvine. She received her PhD in Physics at Princeton University and did postdoctoral work at the University of Illinois at Urbana-Champaign and at Los Alamos National Laboratory. She is a theoretical physicist who does research in condensed matter physics and biophysics. She has studied a wide variety of topics including disordered systems and glasses at low temperatures, phase transitions, noise, superconductors and superconducting qubits, strongly correlated electron systems, developmental biology, intracellular transport and cancer. She is a fellow of the American Physical Society, the American Association for the Advancement of Science, and the American Academy of Arts and Sciences.